Desalination and Water Treatment
www.deswater.com

doi: 10.5004/dwt.2023.29987

308 (2023) 170–182
October

Lignite-derived graphite synthesis for the removal of nonylphenol ethoxylate

Pinar Sevim Elibol[a,*], Hakki Erdogan[b]

[a]*Department of Environmental Engineering, Engineering Faculty, Duzce University, Konuralp Campus, Düzce, Türkiye, email: pinarsevim@duzce.edu.tr*
[b]*Composite Material Technologies, Institute of Science and Technology, Duzce University, Konuralp Campus, Duzce, Türkiye, email: herdogan@duzce.edu.tr*

Received 3 July 2023; Accepted 19 September 2023

ABSTRACT

This research was centred on the synthesis and characterization of lignite-derived graphite (LDG) as an alternative adsorption material for eliminating nonylphenol ethoxylate (NPE) from aqueous solutions. The characterization of LDG revealed distinctive morphological traits, consisting of tubular structures and densely packed layers. These structural attributes augment adsorption capacity when compared to traditional materials by increasing surface area and establishing intricate pathways that facilitate NPE transport. To achieve this goal, the impacts of variables such as pH, contact time, initial concentration, and temperature on NPE removal via LDG were investigated. The study indicated that NPE adsorption onto LDG occurs rapidly, with equilibrium attained within a mere 5 min. Moreover, it was determined that LDG effectively operates across a broad pH range. The acquired data were elucidated using the pseudo-second-order kinetic model, providing the most accurate representation of the adsorption process. Furthermore, the Dubinin–Radushkevich isotherm analysis indicated the prevalence of a physical mechanism in the NPE adsorption onto LDG. Throughout the study, characterization of the synthesized LDG was carried out through X-ray diffraction, scanning electron microscopy, and Brunauer–Emmett–Teller analysis. In conclusion, this study underscores the synergy between LDG's distinctive physical and chemical properties, positioning it as a promising material for efficiently extracting NPE from contaminated water sources.

Keywords: Nanocomposite; Eco-friendly water treatment; Lignite-derived graphite; Nonylphenol ethoxylate; Adsorption

1. Introduction

Endocrine-disrupting chemicals (EDCs) have emerged as a prominent environmental concern in recent years, primarily due to their inherent persistence, potential for bioaccumulation, and capacity to interfere with the endocrine system of both humans and animals [1,2]. Xenoestrogens, a subgroup of EDCs, can be attributed to various sources, including agricultural, industrial, and waste disposal activities, with notable examples being polychlorinated biphenyls (PCBs) and dioxins [3]. Among the xenoestrogens, nonylphenol ethoxylates (NPEs) represent a specific class characterized as non-ionic surfactants [4]. Due to their favorable chemical properties and cost-effectiveness, NPEs have been widely used in various sectors including industry, households, agriculture, and commerce. Their functional utility encompasses roles as antistatic agents, demulsifies, emulsifiers, wetting-dispersing agents, detergents, and solubilizers. Notably, NPEs have achieved significant market penetration, with previous estimates indicating that they constitute approximately 80% of detergent usage [5]. This statistic serves as a testament to the wide-ranging adoption and utilization of NPEs in various domains.

The use of NPEs results in their release into the environment through wastewater pathways [6]. Consequently, NPEs have the potential to enter water bodies or wastewater

* Corresponding author.

treatment plants (WWTPs) [7]. The occurrence of NPEs in water ecosystems, including rivers, lakes, and groundwater, has been documented in previous studies [5,7–9]. This presence poses a significant concern due to the toxic and estrogenic effects NPEs can have on fish and other aquatic organisms [7,10]. Even when NPEs reach WWTPs, conventional treatment systems lack the capacity to effectively eliminate EDCs [11]. Moreover, NPEs have the potential to undergo biodegradation in both the environment and WWTPs, leading to the formation of more toxic compounds. These degradation products may exhibit increased persistence in aquatic environments and become involved in the water cycle [12,13]. Consequently, it is imperative to implement appropriate treatment measures for NPEs and their degradation products to mitigate their potential highly toxic effects on both human health and ecosystems before their release into the environment [14].

The adsorption process has garnered significant attention in wastewater treatment as an effective method for removing pollutants. This is due to its simplicity, cost-effectiveness, and high removal efficiencies achieved [15–19]. A wide range of natural and synthetic adsorbents, such as sand [20], clay [21], biochar [22], aminated adsorbents [23], multi-walled carbon nanotubes [15], polyurethane foam [24], and graphene oxide [25] have been utilized for removing NPEs from aqueous solutions.

Previous investigations have demonstrated that the adsorption of NPEs onto these adsorbent materials is primarily governed by both the hydrophobic and hydrophilic regions of the NPE molecules [20,21,26]. Specifically, the oxygen present in the oxyethylene group within the structure of NPEs interacts with the surface of the adsorbent, facilitating the strong adsorption of the ethoxylated nonionic segment onto the surface [27]. These findings provide insights into the mechanisms underlying the adsorption process and highlight the potential of utilizing adsorbents for the effective removal of NPEs from aqueous environments.

Graphite, recognized as the most thermodynamically stable form of carbon, is composed of graphene layers interconnected by covalent and metallic bonds [28]. When subjected to thermal or chemical treatments, graphite undergoes expansion, resulting in the formation of expanded graphite, which exhibits a remarkable adsorption capacity for organic pollutants [29,30]. The superior adsorption performance of expanded graphite can be attributed to its distinctive physical and chemical properties, including porosity, specific surface area, density, and hydrophobic structure [19,29,31,32].

Natural flake graphite is commonly used as a starting material for the production of expanded graphite. It is treated with graphite intercalation compounds (GICs), such as alkali metals and acids, to achieve the desired expanded form [33–35]. However, the separation and purification processes required to attain the desired purity level of natural graphite are intricate and contribute to increased production costs [36]. As an alternative, coal-based graphite materials have been employed, although their widespread application in the field of wastewater treatment may be hindered by the reliance on high-grade coals such as anthracite and bitumen [37–41]. Limited research has explored the use of low-grade coal in graphite production [42,43].

Lignite, characterized by its high moisture and oxygen content, low calorific value, and susceptibility to spontaneous combustion, represents the lowest grade of coal [44]. However, lignite possesses a porous structure that offers potential for effective pollutant adsorption [45–48]. Previous studies have demonstrated the production of activated carbon, a widely utilized adsorbent material, from lignite [43,47,49,50]. This indicates that lignite could serve as a promising and cost-effective raw material for synthesizing graphite with a highly porous structure. Although previous studies have focused on alternative materials for NPE adsorption, NPEs removal with lignite-derived graphite has not been studied.

In this study, we assessed the novel application of lignite-derived graphite, referred to as lignite-derived graphite (LDG), as an alternative material for removal of nonylphenol ethoxylates (NPEs) in aqueous solutions, marking the first instance of such evaluation in the literature. To achieve this, we initially synthesized LDG using electrochemical techniques, incorporating sulfuric acid, and subsequently conducted comprehensive characterization studies. Subsequently, we explored LDG's capacity for adsorbing Tergitol NP-10 from aqueous solutions, a novel investigation within the existing body of literature.

2. Materials and methods

2.1. Chemicals and instruments

The NPE-based surfactant, Tergitol NP-10 ($C_{35}H_{64}O_{11}$), was acquired from Toronto Research Chemicals (North York, ON, Canada). This product was in the form of a colorless viscous oil that exhibited high solubility in water. A stock solution of NPE at a concentration of 1,000 mg/L was prepared by dissolving Tergitol NP-10 in deionized water (DIW) and subsequently diluted to the desired concentrations prior to use. The DIW used for solution preparation was obtained from the Smart2Pure™ Water Purification System manufactured by Thermo Fisher Scientific Inc., (Waltham, MA, USA). Sulfuric acid (H_2SO_4) and sodium hydroxide (NaOH) were procured from Sigma-Aldrich (Saint Louis, MO, USA). Lignite was ground and sieved to achieve a particle size smaller than 100 mesh, serving as the initial precursor for the production of graphite originating from lignite (LDG).

The concentration of NPE solutions was determined using a high-performance liquid chromatography (HPLC) system consisting of a Shimadzu LC-20AT instrument equipped with a photodiode array detector (Shimadzu SPD-M20A). NPE analysis was conducted using a reversed-phase column, specifically the Inertsil ODS-3 (250 mm × 4.6 mm, 5 μm particle size) from GL Sciences. The mobile phase employed was a mixture of ACN and 0.05 M ammonium acetate (90:10, v/v), flowing at a rate of 1.0 mL/min. The injection volume was set at 50 μL, and the absorbance wavelength was fixed at 227 nm. The concentration of the NPE solution was determined by calculating the peak areas using external calibration standards, with a detection limit below 0.080 mg/L.

2.2. Synthesis of lignite-derived graphite

Lignite can be oxidized to graphite at the surface of the anode located at the center of the cell in the presence of sulfuric acid (H_2SO_4). The application of current enables the intercalation of hydrogen sulfate HSO_4^- and H_2SO_4 into the porous structure of lignite. The reaction of carbon in lignite and HSO_4^- and H_2SO_4 gives graphite bisulfate, according to the Eq. (1).

$$24nC + 3H_2SO_4 \rightarrow C_{24n}^{+} \cdot HSO_4^- \cdot 2H_2SO_4 + H^+ + e^- \quad (1)$$

Lignite-derived graphite (LDG) was synthesized using a previously established electrochemical method [51,52] with a slight modification. Briefly, an electrolytic cell was divided into two sections (anode and cathode) by a membrane. The anode, located at the center of the electrolytic cell, was constructed from graphite. Cathode at the sides of the cell was steel. The electrolytic cell operated in batch mode and the synthesis of LDG was carried out at 18°C–2°C under atmospheric conditions.

The suspension formed after synthesis was transferred into a glass container and mixed with deionized water at 15°C–18°C for hydrolysis. The suspension underwent filtration, and the solid phase was washed with distilled water until the pH reached a range of 5–7. The solid material was then dried at 85°C for 24 h and subjected to calcination at 950°C to produce LDG. Samples were cooled down to room temperature and transferred into screw cap vials for storage.

2.3. Characterization of lignite-derived graphite

Surface morphology of LDG was investigated with scanning electron microscopy (SEM) using Quanta FEG 250 (FEI Company, Hillsboro, OR, USA). TriStar II Plus (Micromeritics Instrument Corporation, Norcross, GA, USA) was used for determination total pore volume, pore-size distribution, and surface area of LDG by using nitrogen adsorption–desorption method. Pore volume and surface area were determinate by applying the p/p_0 = 0.95 to the adsorption data and using Brunauer–Emmett–Teller (BET) equation, respectively. The Barrett–Joyner–Halenda (BJH) method was employed for calculation of the pore-size distribution. X-ray diffraction (XRD) patterns of the LDG were obtained using an automated SmartLab (Rigaku Corporation, Tokyo, Japan) instrument with Cu K-β radiation at 40 kV and 30 mA over the range (2θ) of 10°–90°, at a scanning speed at 5°/min.

2.4. Adsorption experiments

Adsorption studies were conducted in batch reactors at temperatures of 15°C, 25°C, and 35°C. LDG (3 mg/mL) was mixed with 250 mL of Tergitol NP-10 solution at various concentrations (400, 200, 100, 50 and 10 mg/L) in Erlenmeyer flasks. The flasks were sealed with glass stoppers and shaken at 215 rpm for 120 min. Samples were collected at regular intervals and promptly filtered through 0.45 μm membrane syringe filters (Chromafil, Macherey-Nagel, Düren, Germany) to determine the remaining NPE concentration in the aqueous phase. All experiments were performed in triplicate.

The optimization of key parameters for the adsorption process was conducted as follows: The impact of pH on the adsorption of Tergitol NP-10 was investigated within a pH spectrum ranging from 2 to 10 at a constant temperature of 25°C. The concentration of the NPE solution was maintained at 100 mg/L, while the pH of the solution was adjusted using either 0.1 M H_2SO_4 or 0.1 M sodium hydroxide (NaOH) to achieve the desired pH levels. Furthermore, the study assessed the influence of initial Tergitol NP-10 concentrations, which were set at 10, 50, 100, 200, and 400 mg/L, to elucidate their effect on the adsorption process. Throughout these experiments, the LDG dosage remained constant at 1.2 mg/mL. In addition, the research delved into the adsorption characteristics of Tergitol NP-10 onto LDG across a temperature range spanning 15°C, 25°C, and 35°C. The experimental conditions for this phase involved a consistent LDG dosage of 3 mg/mL, an initial NPE concentration of 100 mg/L, a pH level of 6, and an adsorption duration of 120 min. These experiments represent the optimization of parameters for our study.

For kinetic studies, the adsorption experiments were conducted at pH 6 and 25°C under continuous stirring, using an LDG dosage of 1.2 mg/mL and Tergitol NP-10 dosages of 50, 100, 200, and 400 mg/L. The samples were taken at 0, 0.5, 1, 2, 3, 5, 10, 15, 30 and 120 min.

The NPE adsorption capacity (q_e, mg/g) of LDG was calculated using Eq. (2):

$$q_e = \left(\frac{C_0 - C_e}{m}\right) \times V \quad (2)$$

where C_0 is initial concentration, C_e is equilibrium concentration of Tergitol NP-10 (mg/L), m is the mass of adsorbent (g) and V is the volume of the solution (L).

3. Result and discussion

3.1. Characterization of lignite-derived graphite

XRD patterns of lignite-derived graphite (LDG) is illustrated in Fig. 1 showing the effect of treating lignite with concentrated sulfuric acid resulted with graphitization revealed. The relatively weak peak observed in lignite, along with the characteristic diffraction peak at 2θ = 25.65°, can be attributed to the abundance of disordered structures, amorphous carbons, and the unique composition of lignite [53,54]. In contrast, LDG exhibits a sharp diffraction peak at 2θ = 26.48° representing the original ideal graphite crystal [55]. The basal peak (002) at 26° remains nearly in the same position for LDG as observed in lignite. The electrochemical treatment of lignite results in significant crystallization, as indicated by the pronounced and sharp (002) peak observed in lignite-derived graphite (LDG). Furthermore, the (10) band undergoes division, resulting in distinct (100) and (101) peaks, while the emergence of (004) and (110) peaks further confirm the crystalline transformation in lignite [54,56]. The high peak density can be attributed to the increased surface area of LDG compared to lignite.

The carbon crystal layer in the lignite did not undergo any change during intercalation and the number of layers also increased [57,58].

In order to illustrate the impact of the electrochemical treatment on the morphological and surface area characteristics, a SEM analysis was conducted, and the accompanying images can be observed in Fig. 2. Morphology of lignite presented a rough surface (Fig. 2a), while LDG obtained as a result of electrochemical treatment resulted in tubular formations (Fig. 2b). Tubular formations that comprise of packed layers can provide higher surface area and channels to facilitate the transport of pollutants. These formations might have a fast and high-efficiency adsorption rate.

In the case of solid adsorbents, the primary location for adsorption is the interface, with the surface area playing a critical role in determining the adsorption performance. Therefore, we conducted an exploration of the pore parameter characteristics of the lignite-derived graphite material using low-temperature nitrogen adsorption. Also, the BET equation was employed to calculate various parameters related to the porosity of the materials while the pore-size distribution was determined using the BJH method.

BET surface area, pore-volume and average pore size of the lignite were 11.86 m^2/g, 0.013 cm^3/g and 44.37 Å, respectively. After the electrochemical process, the surface area and pore volume of the lignite increased by 8 and 4.7 times, respectively. In contrast, the average pore size decreased by 42%. These changes in pore characteristics are likely attributed to the release of intercalated compounds during the electrochemical processing [59,60]. The pore-size distribution data (Fig. 3b) further support the presence of a porous structure and, with lignite-derived graphite exhibiting a higher average diameter and incremental pore volume compared to lignite. These findings align with the enhanced adsorption capacities observed for lignite-derived graphite throughout the entire range of relative pressures.

The adsorption isotherms for both lignite and lignite-derived graphite displayed typical Type II behavior, indicative of multilayer adsorption on a nonporous or microporous surface [61]. The adsorption capacities increased gradually with the relative pressure, suggesting a progressive adsorption process. Hysteresis loops were observed in the desorption isotherms, indicating the presence of mesopores and capillary condensation effects [41,62].

Comparative analysis of the lignite-derived graphite exhibited significantly higher adsorption capacities across the entire range of relative pressures when compared to lignite (Fig. 3a). This enhancement in adsorption performance can be attributed to the electrochemical treatment and graphitization process, which result in the development of an ordered and porous structure [41]. The increased surface area and pore volume of lignite-derived graphite contribute to its improved adsorption characteristics. Moreover, the desorption data for lignite-derived graphite exhibited reversible adsorption–desorption behavior, indicating its ability to release the adsorbed molecules. In contrast, the desorption data for lignite showed a gradual decrease, suggesting some irreversible adsorption or stronger surface interactions [37]. The obtained results underscore the efficacy of the electrochemical treatment and graphitization of lignite in producing lignite-derived graphite with enhanced adsorption capabilities. These results underscore the efficacy of the electrochemical treatment and graphitization of lignite in producing lignite-derived graphite with enhanced adsorption capabilities. These findings contribute to a better understanding of the structural modifications occurring during the transformation process

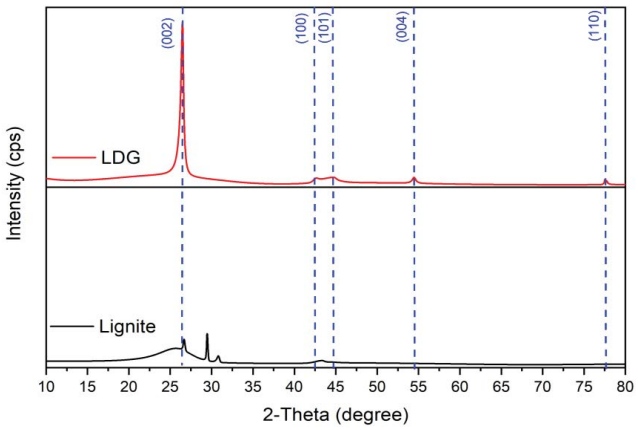

Fig. 1. X-ray diffraction patterns of lignite and lignite-derived graphite (LDG).

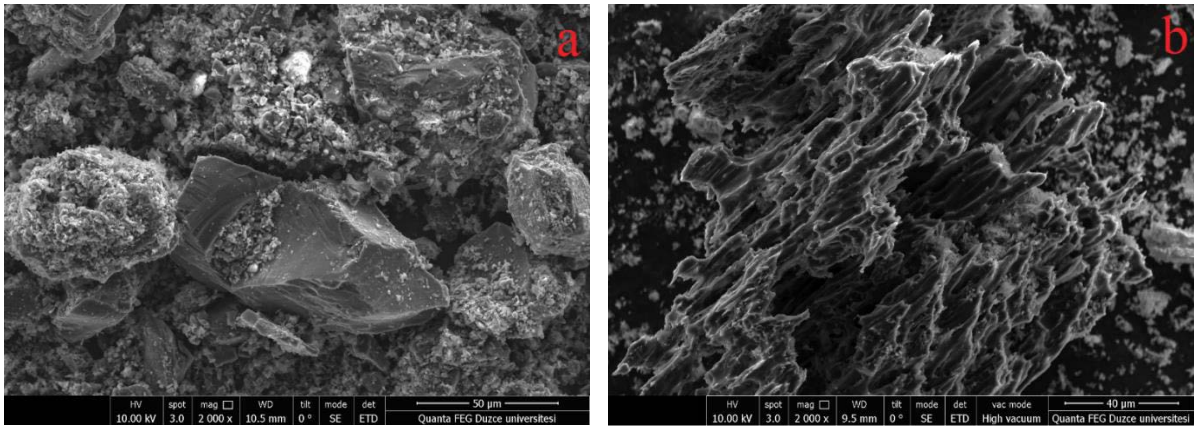

Fig. 2. Scanning electron microscopy images (a) lignite and (b) LDG.

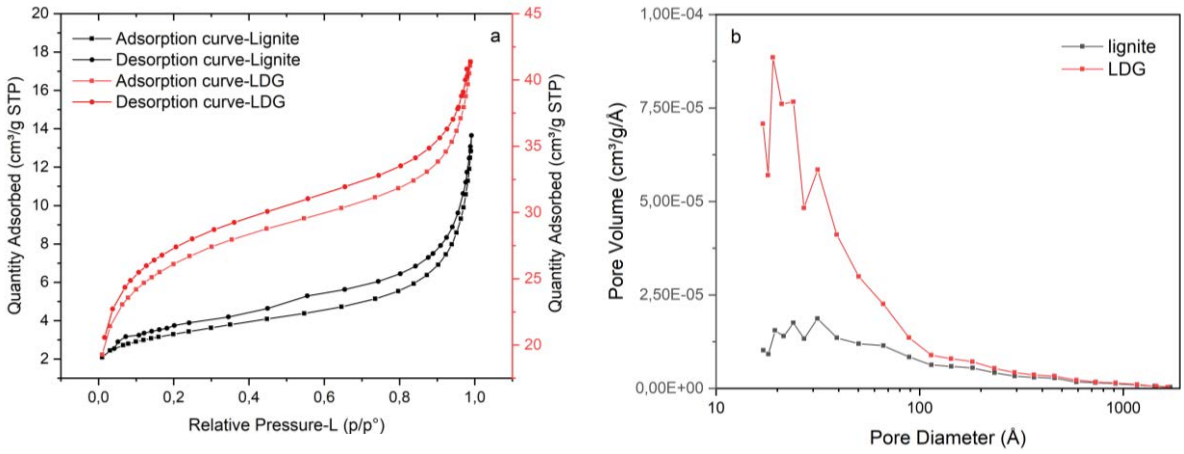

Fig. 3. N_2 adsorption–desorption isotherms (a) and pore-size distribution curves (b) of lignite and LDG.

and highlight the potential of lignite-derived graphite as a promising adsorbent in various applications [40,50,54].

3.2. Studies on the effective parameters on the adsorption of NPE onto LDG

3.2.1. Effect of pH

Fig. 4 illustrates the percentage of nonylphenol ethoxylate (NPE) removal and its adsorption by lignite-derived graphite (LDG) as a function of the pH of the NPE solutions. The results indicated that the adsorption of NPE by LDG remained unaffected by the pH within the range of 2.0 to 10.0. The adsorption capacity of NPE ranged from 15.04 to 16.59 mg/g, with the percentage removal varied between 89.09% and 99.47%. However, there was a slight decrease in NPE adsorption observed at pH levels of 8.0 and 10.0. The highest adsorption capacity of 16.89 mg/g was observed at a slightly acidic pH of 6.0. These findings demonstrate that LDG exhibits efficient NPE adsorption across a broad pH range.

The research conducted by Chen et al. [63] supports our findings, as they investigated the adsorption of non-ionic aromatic compounds using carbon-based absorbents. Their study revealed that the adsorption of hydrophilic compounds with high K_{ow} values remained consistent across different pH ranges. This observation aligns with the outcomes of our present study. It is postulated that the functional groups present on the carbon-based absorbent undergo modifications in response to changes in the pH of solution. These alterations enable the binding of non-ionic compounds through both hydrophilic groups and hydrophobic tails [64,65]. This analysis highlights the pH-independent adsorption behavior of LDG towards NPE, corroborating the potential application of LDG as an effective adsorbent for NPE removal within a wide pH range.

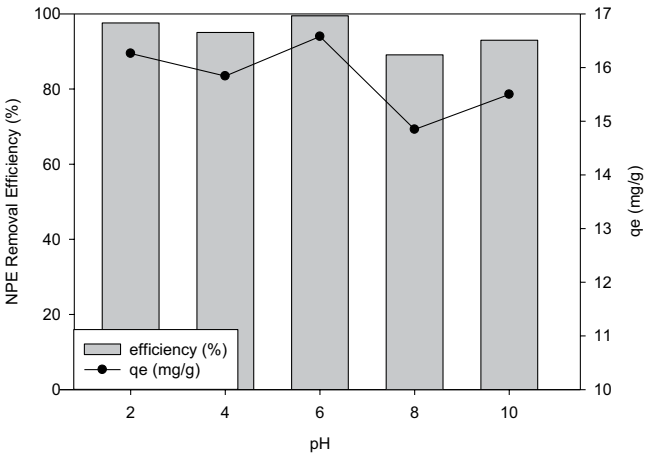

Fig. 4. Effect of pH on the adsorption of NPE onto LDG (LDG dosage: 3 mg/mL; initial NPE concentration: 100 mg/L; reaction time: 120 min).

3.2.2. Effect of temperature

The adsorption behavior of nonylphenol ethoxylate (NPE) onto LDG at different temperatures is presented in Fig. 5, specifically at 15°C, 25°C, and 35°C. The

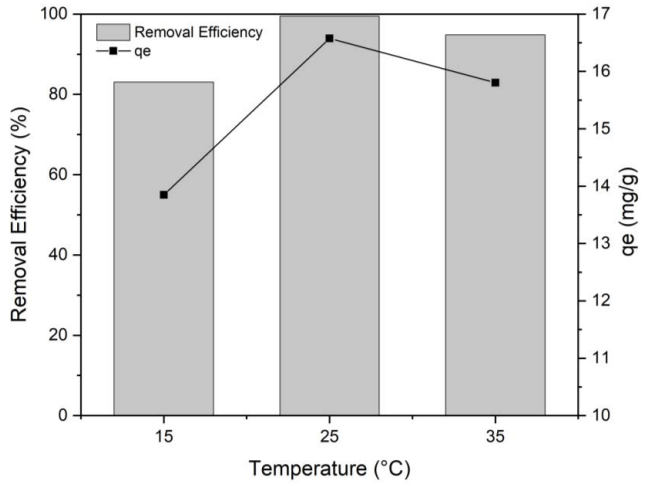

Fig. 5. Effect of temperature on the adsorption of NPE onto LDG (LDG dosage: 3 mg/mL; initial NPE concentration: 100 mg/L; reaction time: 120 min; pH 6).

adsorption capacities were determined to be 13.85, 16.58, and 15.81 mg/g, respectively. It was observed that as the temperature increased from 15°C to 25°C, the percentage removal of NPE rose from 83.01% to 99.46%. This increase can be attributed to the enhanced formation of hydrogen bonds between the hydrophilic group of NPE and water at higher temperatures, while the affinity between the epoxy group and water weakened [64]. However, a slight decrease in adsorption, reaching 94.8%, was observed at 35°C. The decrease in adsorption between 25°C and 35°C, which is possibly due to the large molecular weight of the adsorbate NPE and can be explain by the alteration in the distribution of the adsorbed surfactant on the surface of the absorbent [66]. Vo and Papavassiliou [66] focus on effects of temperature and shear on the adsorption of surfactants on carbon nanotubes, it was demonstrated that an increase in temperature resulted in a change in the distribution of the adsorbed surfactant on the absorbent surface, leading to a decrease in surfactant adsorption from 0.47 mg/g at 25°C to 0.45 mg/g at 40°C. In another study about adsorption of bulky molecules of nonylphenol ethoxylate on ordered mesoporous carbons, increasing adsorption temperature from 20°C to 40°C had been resulted in a slightly decreased NPE uptake for most of the carbon samples in the whole range of equilibrium concentration [67].

According to the principles of kinetic theory, the temperature of an object reflects the average energy of motion (kinetic energy) possessed by its individual particles. This energy is influenced by two factors: the mass of the particles and their speed. In other words, when we maintain a constant temperature, particles with higher molecular weight move at slower speeds, and vice versa. In the context of our study, this concept explains why the adsorption capacity slightly decreased when temperature increased. In a related study, p-nitrophenol which is a smaller molecule was used, as a probe to investigate its adsorption onto activated carbon fiber at various temperatures. Interestingly, they observed that as the temperature decreased, the amount of p-nitrophenol adsorbed onto the activated carbon fiber significantly increased [68]. This finding supports the hypothesis we discussed earlier.

3.2.3. Effect of contact time

The influence of contact time on the adsorption of nonylphenol ethoxylate (NPE) onto LDG was investigated by varying the contact times from 2 to 30 min, and the results are depicted or first 10 min in Fig. 6. It was observed that the adsorption capacity of NPE onto LDG reached a plateau after 5 min, indicating the establishment of equilibrium. This indicates that the adsorption process between NPE and LDG was exceptionally rapid compared to the reported equilibrium time of 14 h for the adsorption of nonylphenol onto multiwalled carbon nanotubes [15].

The rapid attainment of equilibrium within a short contact time suggests that LDG has a high affinity for NPE adsorption. This characteristic is beneficial in practical applications where fast adsorption kinetics are desired for efficient removal of NPE from aqueous solutions. The findings highlight the potential of LDG as an effective adsorbent for the rapid removal of NPE contaminants from water sources.

3.2.4. Effect of initial concentration

The adsorption behavior of nonylphenol ethoxylate (NPE) onto lignite-derived graphite (LDG) was assessed over a range of initial NPE concentrations (50–400 mg/L), and the results are depicted in Fig. 7. It was observed that the equilibrium adsorption of NPE onto LDG increased from 4.14 to 17.18 mg/g as the initial NPE concentration increased from 50 to 400 mg/L. This can be primarily attributed to the heightened concentration gradient between LDG and NPE, resulting in enhanced NPE adsorption [69]. Thus, it can be concluded that the adsorption of NPE is positively influenced by increasing the initial NPE concentration. However, with the increase in the initial NPE concentration from 50 to 400 mg/L, the percentage removal of NPE decreased from 99.26% to 51.16%. This can be attributed to the saturation of available adsorption sites on LDG by NPE molecules [70]. As the concentration of NPE in the solution increases, more NPE molecules compete for the limited adsorption sites, resulting in reduced percentage removal.

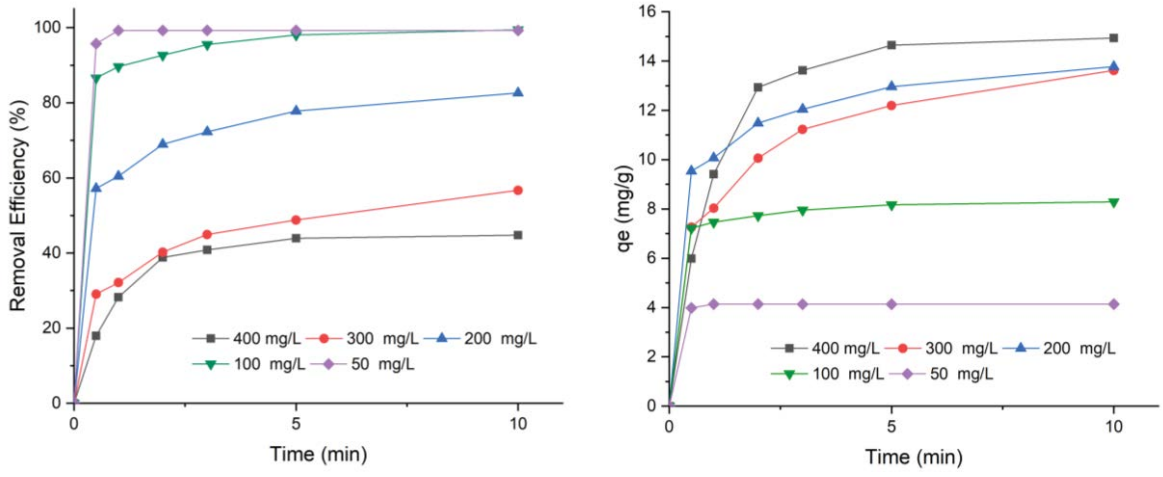

Fig. 6. Effect of contact time on the NPE adsorption by LDG (LDG dosage: 1.2 mg/mL; pH 6).

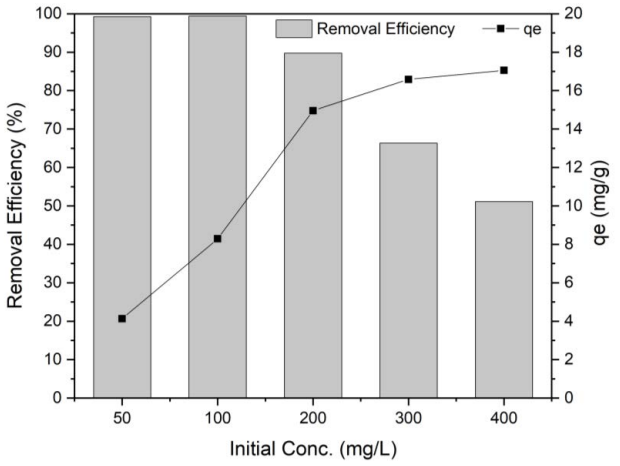

Fig. 7. Effect of initial concentration on the NPE adsorption by LDG (LDG dosage: 1.2 mg/mL g/L; reaction time: 30 min; pH 6).

These findings highlight the importance of considering the initial concentration of NPE when utilizing LDG as an adsorbent for NPE removal. While higher initial concentrations can lead to greater adsorption capacity, the percentage removal may decrease due to the saturation of adsorption sites. Thus, optimizing the initial NPE concentration is crucial for achieving efficient and effective NPE removal using LDG as an adsorbent.

3.3. Adsorption kinetics

The analysis of adsorption kinetics plays a crucial role in determining the adsorption capacity and providing insights into the adsorption mechanism. In this study, the experimental data for the adsorption of nonylphenol ethoxylate (NPE) onto LDG was investigated using several kinetic models, including the pseudo-first-order kinetic model, pseudo-second-order kinetic model, intraparticle diffusion model, and liquid film diffusion model. These models were employed to characterize the kinetic behavior of the adsorption process. The specific equations associated with each kinetic model can be found in Table 1. By examining the data using these models, valuable information regarding the rate of adsorption and the underlying mechanism can be obtained.

The pseudo-first-order kinetic model assumes that the rate of adsorption is directly proportional to the number of available adsorption sites, while the pseudo-second-order kinetic model suggests that the adsorption capacity is proportional to the number of active sites on the LDG [71].

Table 2 presents the correlation coefficients (r^2), parameters, and constants associated with the four kinetic models used to analyze the adsorption of nonylphenol ethoxylate (NPE) onto LDG, while the corresponding kinetic plots can be observed in Fig. 8. Among the four models, the pseudo-second-order kinetic model yielded the highest correlation coefficient ($r^2 > 0.998$) for all initial NPE concentrations. Additionally, it was observed that the experimental equilibrium adsorption capacities (8.17–17.18 mg/g) closely matched the calculated adsorption capacities obtained from the pseudo-second-order kinetic model (8.32–17.40 mg/g).

Table 1
Kinetic models and adsorption isotherms used in present study

Kinetic model	
Pseudo-first-order kinetic model	$\log\left(q_e - q_t\right) = \log q_e - \frac{k_1}{2.303}t$
Pseudo-second-order kinetic model	$\frac{t}{q_t} = \frac{t}{q_e} + \frac{1}{k_2 q_e^2}$
Intraparticle diffusion model	$q_t = k_i t^{1/2} + c_i$
Liquid film diffusion model	$-\ln\left(1-F\right) = k_{fd}t - C$

q_e (mg/g): equilibrium adsorption capacity; q_t (mg/g): the sorption amount at time t; k_1 (min^{-1}): the adsorption rate constant; k_2 (g/mg·min): the rate constant determined by the plots of t/q_t vs. t; k_i (mg/g·min$^{0.5}$): the rate constant; c_i: the intercept related to the thickness of the boundary layer; k_{fd}: the rate constant of liquid film diffusion; C: constant expressed on the boundary layer; F: value is calculated q_t/q_e.

Table 2 provides the k_{fd} and r^2 values associated with the liquid film diffusion model, which suggests that the adsorption kinetics of nonylphenol ethoxylate (NPE) onto LDG are influenced by diffusion through the liquid film surrounding the solid adsorbents. The correlation coefficient values showed an increasing trend with higher NPE concentrations, reaching values of 0.95 and 0.97 for 400 and 300 mg/L, respectively. The experimental data for adsorption kinetics exhibited better fitting with the film diffusion model compared to the intraparticle diffusion model. Notably, the constant expressed on the boundary layer (C) was found to be close to the origin for initial NPE concentrations of 400 and 300 mg/L, measuring 0.85 and 0.63, respectively. This observation suggests that the adsorption kinetics of NPE on LDG may be predominantly controlled by diffusion through the liquid film surrounding the adsorbent particles [72].

3.4. Adsorption isotherms

The adsorption of nonylphenol ethoxylate (NPE) from aqueous solutions onto LDG was characterized using several isotherm models, namely Langmuir, Freundlich, Temkin, and Dubinin–Radushkevich [16,73]. The Langmuir isotherm model is commonly employed to determine the adsorption capacity of various adsorbents by considering the surface coverage and the equilibrium between the adsorbate and adsorbent [74]. The linear equation representing the Langmuir isotherm model is provided in Eq. (3).

$$\frac{C_e}{q_e} = \left(\frac{1}{bq_m}\right) + \left(\frac{1}{q_m}\right) \tag{3}$$

where q_m is the maximum sorption capacity of the absorbent (mg/g), K is the equilibrium constant (L/mg), q_e is the equilibrium adsorption capacity of adsorbate on the adsorbent, C_e is the equilibrium concentration of adsorbate in solution The model coefficients estimated according to the plot of C_e/q_e vs. C_e (Fig. 9b).

Table 2
Kinetic parameters for adsorption of NPE onto LDG

Type	Initial concentration (C_0), 25°C			
	400 mg/L	300 mg/L	200 mg/L	100 mg/L
Experimental q_e (mg/g)	17.18	16.80	14.05	8.17
Pseudo-first-order kinetic model				
q_e (mg/g)	7.35	8.96	5.76	0.52
k_1 (min^{-1})	0.13	0.13	0.05	0.11
r^2	0.95	0.97	0.85	0.89
Pseudo-second-order kinetic model				
q_e (mg/g)	17.40	17.39	15.14	8.32
k_2 (g/mg·min)	0.06	0.04	0.09	1.16
h (mg/g·min)				
r^2	0.999	0.998	0.999	0.9999851
Intraparticle diffusion model				
C	10.82	9.20	10.57	7.68
k_t (mg/g·min$^{1/2}$)	0.79	0.94	0.65	0.08
r^2	0.48	0.61	0.79	0.44
Liquid film diffusion model				
k_{fd}	0.13	0.13	0.05	0.11
C	0.85	0.63	1.06	2.78
r^2	0.95	0.97	0.85	0.65

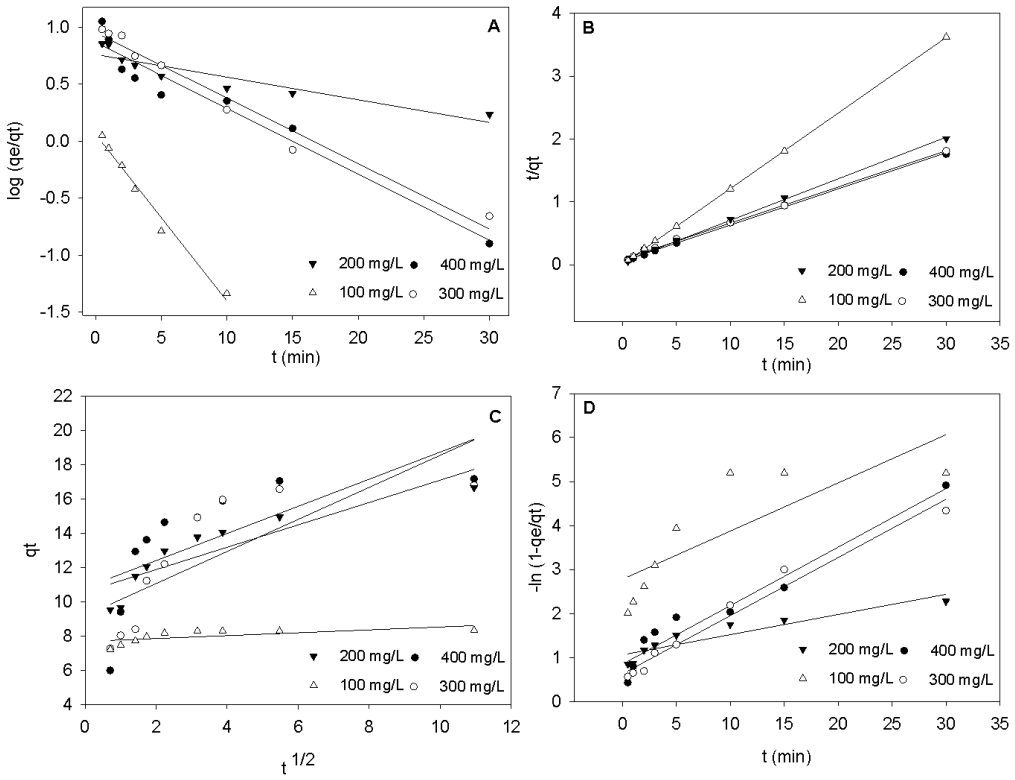

Fig. 8. Kinetic models; pseudo-first-order (a), pseudo-second-order (b), intraparticle diffusion model (c) and liquid film diffusion model (d) for the adsorption of NPE onto LDG (initial concentrations = 100–400 mg/L; 3 mg/mL of LDG; pH 6.0 and 25°C).

Another parameter of the Langmuir isotherm is the separation factor (R_L) given in Eq. (4).

$$R_L = \frac{1}{1 + bC_0} \tag{4}$$

where C_0 is the initial NPE concentration and b (L/g) is the adsorption equilibrium constant and the adsorption process might be linear (R_L = 1), favorable (0 < R_L < 1) or unfavorable (R_L > 1) based on the R_L value [16].

Freundlich isotherm was generally used for the adsorption processes that occur on heterogeneous surfaces [74]. The linear form of the Freundlich equation is given in Eq. (5):

$$\log q_e = \log K_F + \frac{1}{n}\log C_e \tag{5}$$

where q_e is the equilibrium adsorption capacity of adsorbate on the adsorbent, C_e is the equilibrium concentration of adsorbate in solution, K_F is the Freundlich constant (L/mg) and 1/n is the adsorption intensity.

Temkin isotherm is employed for the analysis of the interactions of the adsorbate and adsorbent based on as factor. The linear form of Temkin isotherm can be expressed as:

$$q_e = \frac{RT}{b_T}\ln A + \frac{RT}{b_T}C_e \tag{6}$$

where q_e and C_e is the same expression for Langmuir and Freundlich, b_T is the Temkin constant related to the heat of sorption (kJ/mol) and A is the binding constant at equilibrium, which corresponds to the maximum binding energy (L/g). R is the gas constant (8.314 × 10^{-3} kJ/mol) and T is the absolute temperature (K).

Dubinin–Radushkevich isotherm model is generally applied to express adsorption mechanism with Gaussian energy distribution onto heterogeneous surfaces [74] which can be expressed as in Eq. (7):

$$\ln q_e = \ln q_m - B'\varepsilon^2 \tag{7}$$

where q_m and B' (mol/kJ^2), the model constants. ε represents the Polanyi potential, is defined by Eq. (8):

$$\varepsilon = RT\ln\left(1 + \frac{1}{C_e}\right) \tag{8}$$

$$E = \frac{1}{\sqrt{2B'}} \tag{9}$$

where R represents the gas constant (kJ/mol·K), and T (K) is the temperature. E is free energy required for adsorptive removal is obtained by Eq. (8) and can be used to predict the type of adsorption [75].

In order to comprehend the adsorption mechanism and determine the optimal parameters for the adsorption of nonylphenol ethoxylate (NPE), adsorption isotherm experiments were conducted using LDG. The Langmuir model was applied to analyze the adsorption data and provide insights into the adsorption process. The maximum adsorption capacity (q_m) for LDG, determined using the Langmuir model, was found to be 17.22 mg/g, and it is presented in Table 3 along with the capacities of various other absorbents utilized for the removal of NPE. This value outperforms the adsorption capacity observed in previous studies involving carbon/graphene-based materials [22,76,77]. It's worth noting that certain carbon-based absorbents, like activated carbons derived from safou seeds, can indeed exhibit higher maximum adsorption capacities. However, safou, unlike lignite, which serves as the raw material for LDG, is a locally sourced fruit that isn't readily available in the global market and has very limited potential as a raw material [78]. Another example of materials with greater maximum adsorption capacities is aminated polymeric adsorbents. Nevertheless, it's crucial to take into account that these alternatives can be both labour-intensive and costly when compared to the utilization of LDG [23].

The highest correlation coefficient (r^2) value of 0.9995, compared to other isotherm models, confirmed the suitability of the Langmuir model for NPE removal using LDG as the adsorbent (Fig. 9 and Table 4). The adsorption of NPE on LDG was characterized as monolayer adsorption [16,79], indicating the presence of homogeneous active sites on LDG [80]. The dimensionless separation factor (R_L) was determined to be 0.05, 0.023, 0.013, 0.009, and 0.007 at initial NPE concentrations (C_0) of 50, 100, 200, 300, and 400 mg/L, respectively. These R_L values further confirmed the favorable nature of the Langmuir isotherm model [81,82].

The correlation coefficient (r^2) obtained for the Freundlich isotherm model was determined to be 0.96, which was lower than the r^2 value obtained for the Langmuir isotherm. This suggests that the Freundlich isotherm model was not suitable for describing the adsorption behavior of nonylphenol ethoxylate (NPE). Additionally, the Freundlich isotherm assumes adsorption on heterogeneous surfaces, which may not accurately represent the adsorption process in this case. Hence, it can be concluded that the active adsorption sites on the LDG surface were homogeneous in nature.

The experimental data exhibited good agreement with the Temkin isotherm equation, yielding a high correlation coefficient (r^2) of 0.98. The corresponding parameters

Table 3
Adsorption capacities of absorbents from the literature for the removal of NPE

Absorbant	Absorbent	q_m (mg/g)	References
Aminated polymeric adsorbents	NP-10	51	[23]
Expanded graphite	NP-10	0.26	[76]
Wood charcoal	NP	2.81	[22]
Graphene oxide nanoflakes	4-nonylphenol	10.06	[77]
Activated carbons (safou seeds)	4-nonylphenol	39.490	[78]
Lignite-derived graphite	NP-10	17.22	This study

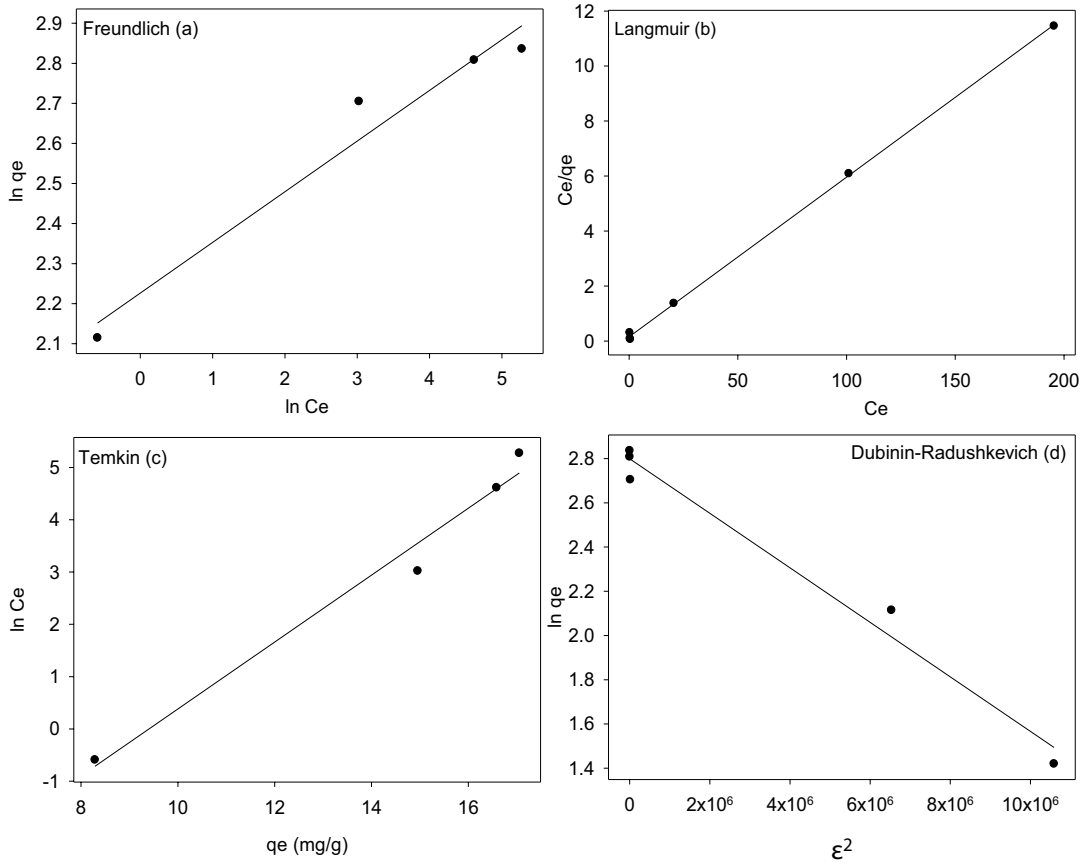

Fig. 9. Adsorption models; Freundlich (a), Langmuir (b), Temkin (c) and Dubinin–Radushkevich (d) plot for adsorption of NPE onto LDG.

Table 4
Isotherm constants for NPE sorption onto LDG

Freundlich isotherm			Langmuir isotherm		
K_F (L/g)	1/n	r^2	q_m (mg/g)	b (L/g)	r^2
168.36	7.90	0.96	17.22	0.38	0.9995
Temkin isotherm			Dubinin–Radushkevich isotherm		
A (L/g)	b_T (kJ/mol)	r^2	K (mol²/kJ²)	q_m (mg/g)	E (kJ/mol)	r^2
4.51	1.62	0.98	1.23×10^{-7}	16.43	2.01	0.98

obtained from the Temkin isotherm were A = 4.51 g/L and b_T = 1.62 kJ/mol. The binding energy calculated was lower than 8 kJ/mol, indicating that the adsorption mechanism involved can be attributed to physical adsorption. Physisorption processes involve weak van der Waals interactions, resulting in relatively low adsorption energies.

The applicability of the Dubinin–Radushkevich isotherm model for the adsorption of nonylphenol ethoxylate (NPE) onto LDG was supported by an r^2 value of 0.98. The Polanyi potential, which is used to determine the adsorption type, was calculated to be 2.01 kJ/mol for the adsorption of NPE onto LDG. According to the Polanyi potential criteria, when E is less than 8 kJ/mol, the adsorption is considered as a physical process, while values between 8 and 16 kJ/mol indicate ion exchange, and E values greater than 16 kJ/mol suggest a chemical adsorption process. In the case of NPE adsorption on LDG, the E value was found to be lower than 8.0 kJ/mol, indicating that the dominant adsorption mechanism was physical adsorption. This conclusion aligns with the findings obtained from the Temkin isotherm model in this study.

4. Conclusion

In conclusion, our study has covered several aspects related to the adsorption of nonylphenol ethoxylate (NPE)

onto carbon-based adsorbents, specifically lignite-derived graphite (LDG). The electrochemical treatment of lignite resulted in the production of LDG, which exhibited improved adsorption properties and favorable pore distribution, including increased mesoporous and microporous regions. The adsorption of NPE by LDG was found to be independent of pH within the range of pH 2.0 to 10.0, with a slight decrease observed at higher pH values. The adsorption capacity of NPE increased with temperature, except at very high temperatures where a slight decrease was observed. Kinetic modeling indicated that the adsorption process followed a pseudo-second-order kinetic model, suggesting chemisorption as the primary mechanism. Isotherm modeling revealed that the Langmuir isotherm provided the best fit to the data, indicating monolayer adsorption on homogeneous active sites. The Temkin isotherm model also showed good agreement, suggesting physical adsorption with low adsorption energies. However, the Freundlich isotherm model was not applicable, suggesting that the adsorption process did not follow a heterogeneous surface. These findings contribute to our understanding of the adsorption behavior of NPE onto LDG and its potential as an effective adsorbent for environmental remediation.

Conflict of interest

The authors declare that they have no conflict of interest.

Acknowledgments

The authors are appreciative for the financial assistance granted by Duzce University, Scientific Research Projects (DUBAP, Project No: 2020.06.02.1087).

Author contributions

Pınar Sevim Elibol designed the research, conducted the experiments, analyzed the data, and wrote the paper. Hakki Erdogan synthesized materials and conducted the experiments.

References

[1] J.L. Wittliff, S.A. Andres, Estrogens V: Xenoestrogens, P. Wexler, Ed., Reference Module in Biomedical Sciences: Encyclopedia of Toxicology (Third Edition), Elsevier, 2014, pp. 480–484. Available at: https://doi.org/10.1016/B978-0-12-386454-3.01018-6
[2] A.C. De la Parra-Guerra, R. Acevedo-Barrios, Studies of endocrine disruptors: nonylphenol and isomers in biological models, Environ. Toxicol. Chem., 42 (2023) 1439–1450.
[3] P.D. Darbre, Environmental Contaminants: Environmental Estrogens - Hazard Characterization, in: Encyclopaedia of Food Safety, Academic Press (Elsevier), Wathem MA, 2014, pp. 323–331. Available at: https://doi.org/10.1016/B978-0-12-378612-8.00196-7
[4] C.L. Yuan, Z.Z. Xu, M.X. Fan, H.Y. Liu, Y.H. Xie, T. Zhu, Study on characteristics and harm of surfactants, J. Chem. Pharm. Res., 6 (2014) 2233–2237.
[5] M. Ahel, W. Giger, C. Schaffner, Behaviour of alkylphenol polyethoxylate surfactants in the aquatic environment—II. Occurrence and transformation in rivers, Water Res., 28 (1994) 1143–1152.
[6] M. Khajvand, P. Drogui, L. Pichon, A. Ali El Khakani, R.D. Tyagi, E. Brien, Removal of nonylphenol ethoxylate from laundry wastewater using modified and functionalized activated carbon, Environ. Sci. Water Res. Technol., 9 (2023) 2338–2354.
[7] G.-G. Ying, B. Williams, R. Kookana, Environmental fate of alkylphenols and alkylphenol ethoxylates—a review, Environ. Int., 28 (2002) 215–226.
[8] J. Newsted, D. Tazelaar, L. Kristofco, B. Losey, A meta-analysis of the occurrence of alkylphenols and alkylphenol ethoxylates in surface waters and sediments in the United States between 2010 and 2020, Environ. Pollut., 330 (2023) 121757, doi: 10.1016/j.envpol.2023.121757.
[9] A. Beryani, K. Flanagan, M. Viklander, G.-T. Blecken, Occurrence and concentrations of organic micropollutants (OMPs) in highway stormwater: a comparative field study in Sweden, Environ. Sci. Pollut. Res., 30 (2023) 77299–77317.
[10] C.-Y. Chen, T.-Y. Wen, G.-S. Wang, H.-W. Cheng, Y.-H. Lin, G.-W. Lien, Determining estrogenic steroids in Taipei waters and removal in drinking water treatment using high-flow solid-phase extraction and liquid chromatography/tandem mass spectrometry, Sci. Total Environ., 378 (2007) 352–365.
[11] P.-D. Nguyen, T.-M.-T. Le, T.-K.-Q. Vo, P.-T. Nguyen, T.-D.-H. Vo, B.-T. Dang, N.-T. Son, D.D. Nguyen, X.-T. Bui, Submerged membrane filtration process coupled with powdered activated carbon for nonylphenol ethoxylates removal, Water Sci. Technol., 84 (2021) 1793–1803.
[12] M. Ahel, C. Schaffner, W. Giger, Behaviour of alkylphenol polyethoxylate surfactants in the aquatic environment—III. Occurrence and elimination of their persistent metabolites during infiltration of river water to groundwater, Water Res., 30 (1996) 37–46.
[13] B. Shao, J. Hu, M. Yang, Nonylphenol ethoxylates and their biodegradation intermediates in water and sludge of a sewage treatment plant, Bull. Environ. Contam. Toxicol., 70 (2003) 527–532.
[14] X. He, B. Yan, J. Jiang, Y. Ouyang, D. Wang, P. Liu, X.-X. Zhang, Identification of key degraders for controlling toxicity risks of disguised toxic pollutants with division of labor mechanisms in activated sludge microbiomes: using nonylphenol ethoxylate as an example, J. Hazard. Mater., 457 (2023) 131740, doi: 10.1016/j.jhazmat.2023.131740.
[15] Y.-D. Dai, K.J. Shah, C.P. Huang, H. Kim, P.-C. Chiang, Adsorption of nonylphenol to multi-walled carbon nanotubes: kinetics and isotherm study, Appl. Sci., 8 (2018) 2295, doi: 10.3390/app8112295.
[16] S. Khandaker, Y. Toyohara, G.C. Saha, Md. Rabiul Awual, T. Kuba, Development of synthetic zeolites from bio-slag for cesium adsorption: kinetic, isotherm and thermodynamic studies, J. Water Process Eng., 33 (2020) 101055, doi: 10.1016/j.jwpe.2019.101055.
[17] M. Sayın, M. Can, M. İmamoğlu, Adsorption of Pd(II) and Au(III) ions by commercial tris(2-aminoethyl) amine polystyrene polymer beads, J. Chem. Eng. Data, 66 (2021) 1132–1143.
[18] F.E. Titchou, R.A. Akbour, A. Assabbane, M. Hamdani, Removal of cationic dye from aqueous solution using Moroccan pozzolana as adsorbent: isotherms, kinetic studies, and application on real textile wastewater treatment, Groundwater Sustainable Dev., 11 (2020) 100405, doi: 10.1016/j.gsd.2020.100405.
[19] M.T. Yagub, T.K. Sen, S. Afroze, H.M. Ang, Dye and its removal from aqueous solution by adsorption: a review, Adv. Colloid Interface Sci., 209 (2014) 172–184.
[20] S. Paria, P.K. Yuet, Adsorption of non-ionic surfactants onto sand and its importance in naphthalene removal, Ind. Eng. Chem. Res., 46 (2007) 108–113.
[21] M. Ghiaci, R.J. Kalbasi, A. Abbaspour, Adsorption isotherms of non-ionic surfactants on Na-bentonite (Iran) and evaluation of thermodynamic parameters, Colloids Surf., A, 297 (2007) 105–113.
[22] L. Lou, Q. Huang, Y. Lou, J. Lu, B. Hu, Q. Lin, Adsorption and degradation in the removal of nonylphenol from water by cells immobilized on biochar, Chemosphere, 228 (2019) 676–684.
[23] J. Fan, W. Yang, A. Li, Adsorption of phenol, bisphenol A and nonylphenol ethoxylates onto hypercrosslinked and aminated adsorbents, React. Funct. Polym., 71 (2011) 994–1000.

[24] Å. Stenholm, M. Hedeland, T. Arvidsson, C.E. Pettersson, Removal of nonylphenol polyethoxylates by adsorption on polyurethane foam and biodegradation using immobilized *Trametes versicolor*, Sci. Total Environ., 724 (2020) 138159, doi: 10.1016/j.scitotenv.2020.138159.
[25] Z. Jin, X. Wang, Y. Sun, Y. Ai, X. Wang, Adsorption of 4-*n*-nonylphenol and bisphenol-a on magnetic reduced graphene oxides: a combined experimental and theoretical studies, Environ. Sci. Technol., 49 (2015) 9168–9175.
[26] D.M. John, W. Alan House, G.F. White, Environmental fate of nonylphenol ethoxylates: differential adsorption of homologs to components of river sediment, Environ. Toxicol. Chem., 19 (2000) 293–300.
[27] R. Zhang, P. Somasundaran, Aggregate formation of binary nonionic surfactant mixtures on hydrophilic surfaces, Langmuir, 21 (2005) 4868–4873.
[28] D.D.L. Chung, Review graphite, J. Mater. Sci., 37 (2002) 1475–1489.
[29] A. Goshadrou, A. Moheb, Continuous fixed bed adsorption of C.I. Acid Blue 92 by exfoliated graphite: an experimental and modeling study, Desalination, 269 (2011) 170–176.
[30] N.B. Hoang, T.T. Nguyen, T.S. Nguyen, T.P.Q. Bui, L.G. Bach, N.D. Duc, The application of expanded graphite fabricated by microwave method to eliminate organic dyes in aqueous solution, Cogent Eng., 6 (2019) 1–13, doi: 10.1080/23311916.2019.1584939.
[31] B. Özmen-Monkul, M.M. Lerner, The first graphite intercalation compounds containing tris(pentafluoroethyl) trifluorophosphate, Carbon N. Y., 48 (2010) 3205–3210.
[32] Y.-P. Zheng, H.-N. Wang, F.-Y. Kang, L.-N. Wang, M. Inagaki, Sorption capacity of exfoliated graphite for oils-sorption in and among worm-like particles, Carbon N. Y., 42 (2004) 2603–2607.
[33] A. Celzard, J.F. Marêché, G. Furdin, Surface area of compressed expanded graphite, Carbon N. Y., 40 (2002) 2713–2718.
[34] H. Horacek, Gaskets with expandable graphite treated with nitric, sulphuric, phosphoric acids and ferric chloride, Open Access Lib. J., 2 (2015) 1–21.
[35] Y. Matsuo, Y. Sugie, Electrochemical lithiation of carbon prepared from pyrolysis of graphite oxide, J. Electrochem. Soc., 146 (1999) 2011, doi: 10.1149/1.1391883.
[36] S. Chehreh Chelgani, M. Rudolph, R. Kratzsch, D. Sandmann, J. Gutzmer, A review of graphite beneficiation techniques, Miner. Process. Extr. Metall. Rev.: An Int. J., 37 (2016) 58–68.
[37] I. Cameán, P. Lavela, J.L. Tirado, A.B. García, On the electrochemical performance of anthracite-based graphite materials as anodes in lithium-ion batteries, Fuel, 89 (2010) 986–991.
[38] I. Cameán, A.B. Garcia, Graphite materials prepared by HTT of unburned carbon from coal combustion fly ashes: performance as anodes in lithium-ion batteries, J. Power Sources, 196 (2011) 4816–4820.
[39] G. Feng, Q. Jiangying, Z. Zongbin, Z. Quan, L. Beibei, Q. Jieshan, A green strategy for the synthesis of graphene supported Mn_3O_4 nanocomposites from graphitized coal and their supercapacitor application, Carbon N. Y., 80 (2014) 640–650.
[40] B. Xing, C. Zhang, Y. Cao, G. Huang, Q. Liu, C. Zhang, Z. Chen, G. Yi, L. Chen, J. Yu, Preparation of synthetic graphite from bituminous coal as anode materials for high performance lithium-ion batteries, Fuel Process. Technol., 172 (2018) 162–171.
[41] Q. Zhou, Z. Zhao, Y. Zhang, B. Meng, A. Zhou, J. Qiu, Graphene sheets from graphitized anthracite coal: preparation, decoration, and application, Energy Fuels, 26 (2012) 5186–5192.
[42] T. Qiu, J.-G. Yang, X.-J. Bai, Y.-L. Wang, The preparation of synthetic graphite materials with hierarchical pores from lignite by one-step impregnation and their characterization as dye absorbents, RSC Adv., 9 (2019) 12737–12746.
[43] S. Shrestha, G. Son, S.H. Lee, T.G. Lee, Isotherm and thermodynamic studies of Zn(II) adsorption on lignite and coconut shell-based activated carbon fiber, Chemosphere, 92 (2013) 1053–1061.
[44] E.M. Suuberg, W.A. Peters, J.B. Howard, Product composition and kinetics of lignite pyrolysis, Ind. Eng. Chem. Process Des. Dev., 17 (1978) 37–46.
[45] C.-X. Pan, X.-Y. Wei, H.-F. Shui, Z.-C. Wang, J. Gao, C. Wei, X.-Z. Cao, Z.-M. Zong, Investigation on the macromolecular network structure of Xianfeng lignite by a new two-step depolymerization, Fuel, 109 (2013) 49–53.
[46] A. Tahmasebi, J. Yu, Y. Han, F. Yin, S. Bhattacharya, D. Stokie, Study of chemical structure changes of chinese lignite upon drying in superheated steam, microwave, and hot air, Energy Fuels, 26 (2012) 3651–3660.
[47] L. Lv, H. Liu, Q. Li, J. Liu, Y. Zhang, Y. Wang, Effective adsorption of Pb(II) from wastewater using facile enclosed pyrolysis strategy for defect-rich lignite-based carbon-coated zero-valent iron, J. Anal. Appl. Pyrolysis, 169 (2023) 105823, doi: 10.1016/j.jaap.2022.105823.
[48] M. Sun, S. Gu, X. Liu, J. Zheng, Z. Xu, Y. Chen, H. He, L. Wang, Adsorption mechanism of ammonia nitrogen and phenol on lignite surface: molecular dynamics simulations and quantum chemical calculations, Fuel, 337 (2023) 127157, doi: 10.1016/j.fuel.2022.127157.
[49] T. Depci, Comparison of activated carbon and iron impregnated activated carbon derived from Gölbaşı lignite to remove cyanide from water, Chem. Eng. J., 181–182 (2012) 467–478.
[50] G. Skodras, Th. Orfanoudaki, E. Kakaras, G.P. Sakellaropoulos, Production of special activated carbon from lignite for environmental purposes, Fuel Process. Technol. 77–78 (2002) 75–87.
[51] J.O. Besenhard, E. Theodoridou, H. Möhwald, J.J. Nickl, Electrochemical applications of graphite intercalation compounds, Synth. Met., 4 (1982) 211–223.
[52] N.E. Sorokina, N.V. Maksimova, V.V. Avdeev, Anodic oxidation of graphite in 10 to 98% HNO_3, Inorg. Mater., 37 (2001) 360–365.
[53] L. Zhao, N. Guanhua, W. Hui, S. Qian, W. Gang, J. Bingyou, Z. Chao, Molecular structure characterization of lignite treated with ionic liquid via FTIR and XRD spectroscopy, Fuel, 272 (2020) 117705, doi: 10.1016/j.fuel.2020.117705.
[54] Y.-M. Wang, C.-H. Zhang, Study on structural evolution of synthetic graphite derived from lignite prepared by high temperature–high pressure method, Crystals, 12 (2022) 464, doi: 10.3390/cryst12040464.
[55] H. Badenhorst, Microstructure of natural graphite flakes revealed by oxidation: limitations of XRD and Raman techniques for crystallinity estimates, Carbon N. Y., 66 (2014) 674–690.
[56] M.S. Nyathi, C.B. Clifford, H.H. Schobert, Characterization of graphitic materials prepared from different rank Pennsylvania anthracites, Fuel, 114 (2013) 244–250.
[57] R. Krishna, J. Wade, A.N. Jones, M. Lasithiotakis, P.M. Mummery, B.J. Marsden, An understanding of lattice strain, defects and disorder in nuclear graphite, Carbon N. Y., 124 (2017) 314–333.
[58] F.M. Uhl, Q. Yao, H. Nakajima, E. Manias, C.A. Wilkie, Expandable graphite/polyamide-6 nanocomposites, Polym. Degrad. Stab., 89 (2005) 70–84.
[59] I.M. Afanasov, O.N. Shornikova, D.A. Kirilenko, I.I. Vlasov, L. Zhang, J. Verbeeck, V.V. Avdeev, G. Van Tendeloo, Graphite structural transformations during intercalation by HNO_3 and exfoliation, Carbon N. Y., 48 (2010) 1862–1865.
[60] R.B. Valapa, G. Pugazhenthi, V. Katiyar, Effect of graphene content on the properties of poly(lactic acid) nanocomposites, RSC Adv., 5 (2015) 28410–28423.
[61] K.S.W. Sing, D.H. Everett, R.A.W. Haul, L. Moscou, R.A. Pierotti, J. Rouquerol, T. Siemieniewska, Reporting physisorption data for gas/solid systems with special reference to the determination of surface area and porosity, Pure Appl. Chem., 57 (1985) 603–619.
[62] X. Li, D. Tan, L. Xie, H. Sun, S. Sun, G. Zhong, P. Ren, Effect of surface property of halloysite on the crystallization behavior of PBAT, Appl. Clay Sci., 157 (2018) 218–226.
[63] J. Chen, W. Chen, D. Zhu, Adsorption of nonionic aromatic compounds to single-walled carbon nanotubes: effects of aqueous solution chemistry, Environ. Sci. Technol., 42 (2008) 7225–7230.

[64] Z. Li, C. Ma, J. Wang, X. Lyu, Q. Zhang, X. You, L. Li, Investigation of nonylphenol ethoxylate on the surface characteristics of low rank coal, Part. Sci. Technol.: An Int. J., 38 (2020) 1012–1018.
[65] T. Svitova, R.M. Hill, C.J. Radke, Adsorption layer structures and spreading behavior of aqueous non-ionic surfactants on graphite, Colloids Surf., A, 183–185 (2001) 607–620.
[66] M.D. Vo, D.V. Papavassiliou, Effects of temperature and shear on the adsorption of surfactants on carbon nanotubes, J. Phys. Chem. C, 121 (2017) 14339–14348.
[67] X. Yuan, W. Xing, S.P. Zhuo, W. Si, X. Gao, Z. Han, Z.F. Yan, Adsorption of bulky molecules of nonylphenol ethoxylate on ordered mesoporous carbons, J. Colloid Interface Sci., 322 (2008) 558–565.
[68] D. Tang, Z. Zheng, K. Lin, J. Luan, J. Zhang, Adsorption of p-nitrophenol from aqueous solutions onto activated carbon fiber, J. Hazard. Mater., 143 (2007) 49–56.
[69] Y.A. Aydin, N.D. Aksoy, Adsorption of chromium on chitosan: optimization, kinetics and thermodynamics, Chem. Eng. J., 151 (2009) 188–194.
[70] M. Zhao, P. Liu, Adsorption of methylene blue from aqueous solutions by modified expanded graphite powder, Desalination, 249 (2009) 331–336.
[71] D. Ursueguía, E. Díaz, S. Ordóñez, Adsorption of methane and nitrogen on basolite MOFs: equilibrium and kinetic studies, Microporous Mesoporous Mater., 298 (2020) 110048, doi: 10.1016/j.micromeso.2020.110048.
[72] Sk. Taheruddin Ahamed, C. Kulsi, Kirti, D. Banerjee, D.N. Srivastava, A. Mondal, Synthesis of multifunctional CdSe and Pd quantum dot decorated CdSe thin films for photocatalytic,electrocatalytic and thermoelectric applications, Surf. Interfaces, 25 (2021) 101149, doi: 10.1016/j.surfin.2021.101149.
[73] A.S. Eltaweil, H. Ali Mohamed, E.M. Abd El-Monaem, G.M. El-Subruiti, Mesoporous magnetic biochar composite for enhanced adsorption of malachite green dye: characterization, adsorption kinetics, thermodynamics and isotherms, Adv. Powder Technol., 31 (2020) 1253–1263.
[74] N. Ayawei, A.N. Ebelegi, D. Wankasi, Modelling and interpretation of adsorption isotherms, J. Chem., 2017 (2017) 3039817, doi: 10.1155/2017/3039817.
[75] S. Mondal, S.K. Majumder, Honeycomb-like porous activated carbon for efficient copper(II) adsorption synthesized from natural source: kinetic study and equilibrium isotherm analysis, J. Environ. Chem. Eng., 7 (2019) 103236, doi: 10.1016/j.jece.2019.103236.
[76] Z. Si-ning, G. Hui, L. Jin-Ming, P. Zhe-min, Absorption of the non-ionic surfactants with expanded graphite, Guangzhou Chem., (2009), doi: 10.16560/j.cnki.gzhx.2009.02.001.
[77] H.N. Catherine, M.-H. Ou, B. Manu, Y.-h. Shih, Adsorption mechanism of emerging and conventional phenolic compounds on graphene oxide nanoflakes in water, Sci. Total Environ., 635 (2018) 629–638.
[78] C.D. Atemkeng, G.S. Anagho, R.F.T. Tagne, L.A. Amola, A. Bopda, T. Kamgaing, Optimization of 4-nonylphenol adsorption on activated carbons derived from safou seeds using response surface methodology, Carbon Trends, 4 (2021) 100052, doi: 10.1016/j.cartre.2021.100052.
[79] H.T. Thi, A. Le Hoang, T.P. Huu, T.N. Dinh, S.W. Chang, W.J. Chung, D. Duc Nguyen, Adsorption isotherms and kinetic modeling of methylene blue dye onto a carbonaceous hydrochar adsorbent derived from coffee husk waste, Sci. Total Environ., 725 (2020) 138325, doi: 10.1016/j.scitotenv.2020.138325.
[80] Y. Liu, Y. Xiong, P. Xu, Y. Pang, C. Du, Enhancement of Pb(II) adsorption by boron doped ordered mesoporous carbon: isotherm and kinetics modeling, Sci. Total Environ., 708 (2020) 134918, doi: 10.1016/j.scitotenv.2019.134918.
[81] K.U. Ahamad, R. Singh, I. Baruah, H. Choudhury, M.R. Sharma, Equilibrium and kinetics modeling of fluoride adsorption onto activated alumina, alum and brick powder, Groundwater Sustainable Dev., 7 (2018) 452–458.
[82] E. Salehi, N. Gavari, A. Chehrei, S. Amani, N. Amani, K. Zaghi, Efficient separation of triglyceride from blood serum using *Cinnamon* as a novel biosorbent: adsorption thermodynamics, kinetics, isothermal and process optimization using response surface methodology, Process Biochem., 77 (2019) 122–136.